

Direct visualization of solute locations in laboratory ice samples

T. Hullar and
C. Anastasio

Direct visualization of solute locations in laboratory ice samples

T. Hullar and C. Anastasio

Department of Land, Air, and Water Resources, University of California, Davis, USA

Received: 29 October 2015 – Accepted: 22 November 2015 – Published: 15 January 2016

Correspondence to: C. Anastasio (canastasio@ucdavis.edu)

Published by Copernicus Publications on behalf of the European Geosciences Union.

Title Page

Abstract

Introduction

Conclusions

References

Tables

Figures

◀

▶

◀

▶

Back

Close

Full Screen / Esc

Printer-friendly Version

Interactive Discussion



Abstract

Many important chemical reactions occur in polar snow, where solutes may be present in several reservoirs, including at the air–ice interface and in liquid-like regions within the ice matrix. Some recent laboratory studies suggest chemical reaction rates may differ in these two reservoirs. While investigations have examined where solutes are found in natural snow and ice, similar research has not identified solute locations in laboratory samples, nor the possible factors controlling solute segregation. To address this, we examined solute locations in ice samples prepared from either aqueous cesium chloride (CsCl) or Rose Bengal solutions that were frozen using several different methods. Samples frozen in a laboratory freezer had the largest liquid-like inclusions and air bubbles, while samples frozen in a custom freeze chamber had somewhat smaller air bubbles and inclusions; in contrast, samples frozen in liquid nitrogen showed much smaller concentrated inclusions and air bubbles, only slightly larger than the resolution limit of our images ($\sim 2\ \mu\text{m}$). Freezing solutions in plastic vs. glass vials had significant impacts on the sample structure, perhaps because the poor heat conductivity of plastic vials changes how heat is removed from the sample as it cools. Similarly, the choice of solute had a significant impact on sample structure, with Rose Bengal solutions yielding smaller inclusions and air bubbles compared to CsCl solutions frozen using the same method. Additional experiments using higher-resolution imaging of an ice sample show that CsCl moves in a thermal gradient, supporting the idea that the solutes in ice are present in liquid-like regions. Our work shows that the structure of laboratory ice samples, including the location of solutes, is sensitive to freezing method, sample container, and solute characteristics, requiring careful experimental design and interpretation of results.

TCD

doi:10.5194/tc-2015-197

Direct visualization of solute locations in laboratory ice samples

T. Hullar and
C. Anastasio

Title Page

Abstract

Introduction

Conclusions

References

Tables

Figures

◀

▶

◀

▶

Back

Close

Full Screen / Esc

Printer-friendly Version

Interactive Discussion



1 Introduction

Snowpacks can be important locations for a variety of chemical reactions, particularly in polar regions (Bartels-Rausch et al., 2014; Domine and Shepson, 2002). Because light can penetrate several tens of cm into the snowpack, photochemical reactions are particularly important (Grannas et al., 2007), including nitrate photolysis forming NO_x (Beine et al., 2002; Jacobi et al., 2004), hydrogen peroxide photolysis to form hydroxyl radical (Chu and Anastasio, 2005; Jacobi et al., 2006), and transformation of organics (Dibb and Arsenault, 2002; Sumner and Shepson, 1999).

A variety of potential chemical reactants have been identified in snowpacks worldwide. Impurities can integrate into snow crystals during formation, or be deposited onto the surface of formed crystals. Reactants and products also partition between the snow crystals and the overlying air; the large surface area of the snow crystals provides an extensive environment for reactions to occur. As the snowpack consolidates, chemical compounds can remain at the surface of the crystals, or become trapped internally at grain boundaries or triple junctions (Domine et al., 2008; Grannas et al., 2007).

There appear to be three reservoirs for impurities in snow: a quasi-liquid layer (QLL) at the ice–air interface; liquid-like regions (LLRs) within the ice (e.g., at grain boundaries); and the bulk ice matrix, i.e., between frozen water molecules (Barret et al., 2011; Grannas et al., 2007; Jacobi et al., 2004). While the exact location of solutes in snow is not well understood (Bartels-Rausch et al., 2014), the location is important for several reasons. First, chemicals present in a surface QLL can be more readily released to the atmosphere compared to impurities segregated into an internal LLR; furthermore, gas-phase oxidants and other species can readily partition from the air onto solutes at the air–ice interface. Second, photon fluxes can vary considerably in various locations within the snowpack (Phillips and Simpson, 2005), and possibly within crystals themselves. Third, the rates of reactions of impurities appear to vary with location. For example, photolysis rates of PAHs can be up to five times faster in surface QLLs compared to in whole ice samples (where PAHs are likely in LLRs) or in aqueous solution

TCD

doi:10.5194/tc-2015-197

Direct visualization of solute locations in laboratory ice samples

T. Hullar and
C. Anastasio

Title Page

Abstract

Introduction

Conclusions

References

Tables

Figures

◀

▶

◀

▶

Back

Close

Full Screen / Esc

Printer-friendly Version

Interactive Discussion

(Kahan and Donaldson, 2007, 2010; Ram and Anastasio, 2009). An investigation of reactions in frozen solutions (Kurkova et al., 2011) suggested the QLL and LLR physical reaction environments are substantially different, with QLLs best represented by a 2-D cage and LLRs as a 3-D cage. This work also found that the cage effect at a given temperature was much more pronounced for reactions occurring in QLLs than LLRs, with solutes in QLLs somewhat surprisingly having less mobility compared to solutes in LLRs.

Because of the potential reactivity differences between the reservoirs, understanding reaction rates in different compartments requires knowing where solutes are located. Solute locations in natural snow and ice samples have been studied using electron microscopy (Barnes et al., 2003; Lomonaco et al., 2009; Rosenthal et al., 2007), and were found to preferentially segregate to grain boundaries and triple junctions. However, we are aware of only one study (Cheng et al., 2010) which directly examined solute location in laboratory snow and ice samples. Instead, solute location is most often inferred from the way the sample is made (Kahan et al., 2010) or from chemical behavior (Kurkova et al., 2011).

The main goal of this paper is to examine the location of solutes in laboratory-prepared frozen solutions. In order to do this, we use X-ray computed tomography (CT), a technique that has been used to create 3-dimensional images of a variety of biological and natural materials (Blanke et al., 2013; Evans et al., 2008). High resolution microCT, which is capable of a spatial resolution of $< 10 \mu\text{m}$, has been used to look at the structure of natural snow and ice (Chen and Baker, 2010; Heggli et al., 2011; Lomonaco et al., 2011; Obbard et al., 2009). But to our knowledge this method has not been used to investigate the structure and solute locations for laboratory samples prepared under controlled conditions with specific solutes.

Thus here we examine the locations of impurities in frozen aqueous solutions prepared in the laboratory. We are primarily interested in the locations of solutes in ices prepared using different freezing methods aimed at putting solutes in specific reservoirs within the ice. In this work we focus on cesium chloride (CsCl) as our solute.

TCD

doi:10.5194/tc-2015-197

Direct visualization of solute locations in laboratory ice samples

T. Hullar and
C. Anastasio

Title Page

Abstract

Introduction

Conclusions

References

Tables

Figures

◀

▶

◀

▶

Back

Close

Full Screen / Esc

Printer-friendly Version

Interactive Discussion



However, because a previous study (Cheng et al., 2010) found different solutes can affect freezing morphology and therefore may influence solute location, we also imaged ice containing the organic compound Rose Bengal. For our samples we present both qualitative (visual) and quantitative results.

2 Methods

We prepared samples by freezing 1.0 mM aqueous solutions of cesium chloride or, in a few cases, 1.0 mM Rose Bengal. High purity water (“Milli-Q water”) was from house-treated deionized water that was run through a Barnstead International DO813 activated carbon cartridge and then a Millipore Milli-Q Plus system. We chose cesium chloride (Sigma-Aldrich, 99.9%) for our primary solute because of its high solubility in water and high X-ray mass attenuation coefficient ($\sim 4.4 \text{ cm}^2 \text{ g}^{-1}$ at 70 keV, NIST, 2015), enabling visualization of low concentrations in our microCT system. We also used Rose Bengal to study the impacts of solute size and polarity on sample morphology. While 1.0 mM of solute is higher than typical solute concentrations in continental (inland) natural snows, it is within the range of concentrations measured in coastal snowpacks (Beine et al., 2011; Douglas and Sturm, 2004; Yang et al., 1996). The chosen concentration allows easy visualization in our system and provides enough material to evaluate spatial patterns in the sample.

We froze most samples as a 500 μL aliquot in a capped glass vial (approximately 3 cm high and 1 cm in diameter, with a total vial volume of $\sim 2 \text{ mL}$) using one of three methods. In the first technique (“Freezer”), we placed samples upright in a laboratory freezer at $\sim -20^\circ\text{C}$; freezing took approximately 1 h. In the second technique (“Freeze Chamber”), we froze samples upright in a custom-built freeze chamber (Hullar and Anastasio, 2011) whose base was cooled to either -10 or -20°C . Typically, the sample sat directly on the base of the freeze chamber surrounded by air. However, we also froze some samples surrounded by drilled metal plates, effectively placing the sample in a metal “well”; the distance between the sample and the surrounding plates was

TCD

doi:10.5194/tc-2015-197

Direct visualization of solute locations in laboratory ice samples

T. Hullar and
C. Anastasio

Title Page

Abstract

Introduction

Conclusions

References

Tables

Figures

◀

▶

◀

▶

Back

Close

Full Screen / Esc

Printer-friendly Version

Interactive Discussion



ple, while including small amounts of top air as sample. Some images presented here were mathematically smoothed by the software, which sometimes resulted in small features ($< 80 \mu\text{m}$ in diameter) being eliminated from movies and still images; however, smoothing did not substantially change the interpretation of our results. In some cases we prepared histograms of the data, which were not smoothed and include all sample data.

To quantitate CsCl concentration in each voxel, we first imaged samples of Milli-Q water, as both liquid and ice, and measured the average radiodensity (image greyscale value) of a subvolume within each sample. As expected, the average radiodensity of ice ($4948 \pm 160 (1\sigma)$) was less than that of liquid water ($5372 \pm 194 (1\sigma)$) due to the lower density of ice. Our measured radiodensity ratio between ice (at -10°C) and water (at 20°C) was 0.921, matching a calculated density ratio from literature values (Haynes, 2014) of 0.921. Next, we imaged 8 aqueous solutions of CsCl at varying concentrations (1.0 mM to 5.0 M) to construct a calibration curve. Plotting these points (Fig. 1) shows a linear relationship between CsCl concentration and measured radiodensity, with a y intercept value within the range of our measured radiodensities for pure liquid water. Therefore, the measured radiodensity of a voxel within a sample containing CsCl in solution (or ice) is linearly related to the amount of CsCl present in the voxel. We assume the relationship between CsCl concentration and radiodensity is the same for ice and water. This allows us to determine the amount of CsCl present in a sample voxel by subtracting the average greyscale value of pure water (or ice) and then using the standard curve to calculate the CsCl mass.

When aqueous solutions are frozen, solutes are generally excluded from the forming ice matrix, resulting in a two distinct components: pure (or nearly pure) water ice, and a concentrated solution of solute (Cho et al., 2002), which can be present at the air-ice interface (i.e., as a QLL) and/or in LLRs within the sample. Freezing-point depression dictates that the solute concentration in these regions is solely a function of the ice temperature (Cho et al., 2002) and is independent of the solute concentration in the initial solution. For example, at -10°C , the predicted total solute concentration in LLRs

Direct visualization of solute locations in laboratory ice samples

T. Hullar and
C. Anastasio

Title Page

Abstract

Introduction

Conclusions

References

Tables

Figures

◀

▶

◀

▶

Back

Close

Full Screen / Esc

Printer-friendly Version

Interactive Discussion



is 5.4 M of solute ions, or 2.7 M of a binary salt such as CsCl. This LLR concentration is considerably lower than the solubility limit of CsCl (11.1 M at 20 °C, NIH, 2015), but higher than the solubility limit of Rose Bengal (1 mM, temperature not given, Neckers, 1989). Therefore, we do not expect CsCl to precipitate, although Rose Bengal might.

As described earlier, we use the Fig. 1 calibration curve to convert microCT greyscale values of radiodensity for each voxel to the mass of solute in each voxel. While this mass could be expressed as an equivalent concentration in the voxel, we believe it is more accurate to consider each voxel as a mixture of pure water ice (with zero solute) and LLRs (regions with a total solute ion concentration of 5.4 M at -10 °C, equivalent to a CsCl concentration of 2.7 M). Thus we express the composition of each voxel as the fraction of voxel volume occupied by liquid-like regions, V_{LLR}/V_{VOXEL} :

$$\frac{V_{LLR}}{V_{VOXEL}} = \frac{(RD_{MEAS} - RD_{ICE})/Slope}{2.7M} \quad (1)$$

where V_{LLR} is the LLR volume, V_{VOXEL} represents the volume of the entire voxel, RD_{MEAS} is the measured radiodensity of the voxel, RD_{ICE} is the radiodensity of pure ice, and Slope is the measured slope of the standard curve line ($10\,409\text{ M}^{-1}$; Fig. 1). A voxel containing only pure ice has $V_{LLR}/V_{VOXEL} = 0$, while a voxel composed entirely of 5.4 M total solute in water has $V_{LLR}/V_{VOXEL} = 1$.

For clarity, we have segmented many of our images into four domains: voxels containing air (defined as $V_{LLR}/V_{VOXEL} < -3.4\%$), voxels containing ice and little or no solute ($V_{LLR}/V_{VOXEL} = -3.4$ to 2%), voxels with 2–10% of volume as LLRs, and voxels with more than 10% of their volume occupied by LLRs. We define an “air” voxel as having a radiodensity less than or equal to the average radiodensity of an imaged air sample, i.e., 3996. As noted above, greyscale values from images of pure materials vary somewhat, meaning a clear distinction between two materials with similar average greyscale values is not possible. We chose to set the cutoff for segmenting LLRs at 2%, a greyscale value of 5507, since this threshold is three standard deviations greater than the average greyscale value for pure ice, which will essentially eliminate

Direct visualization of solute locations in laboratory ice samples

T. Hullar and
C. Anastasio

Title Page

Abstract

Introduction

Conclusions

References

Tables

Figures

◀

▶

◀

▶

Back

Close

Full Screen / Esc

Printer-friendly Version

Interactive Discussion



the problem of identifying water ice as solute. Because of this high threshold it is quite likely that solute is present in some voxels characterized as “ice”. On the other hand, voxels defined as having an LLR percentage of 2 % or greater almost certainly contain solute. For some samples, we calculated the mass of CsCl present in each domain.

5 As the mass of CsCl present in the water ice domain could not be determined directly, we assumed any mass not present in either the LLR 2–10 % or LLR > 10 % domains is present in the “ice” domain.

3 Results and discussion

We first present imaging results for samples prepared without added solute (frozen Milli-Q water). Figure 2a shows a reconstructed image of a “pure” ice sample prepared by freezing air-saturated Milli-Q in a glass vial in a laboratory freezer; the full movie, which shows the sample rotating, is in Fig. S1 in the Supplement. Air bubbles are visible as light grey spheroids, and are generally located towards the center of the sample, away from the vial walls and base. This is likely because the entire outer surface of the vial was cooled and, because glass has a higher thermal conductivity than liquid water, the water apparently froze from the outside inward.

15 Figure 2b shows a reconstruction of a similar Milli-Q sample, but now where the solution was degassed with helium for 30 min before freezing; the full movie is in Fig. S2 in the Supplement. Because He degassing replaces the more soluble nitrogen and oxygen in the air-saturated solution with less soluble helium, fewer bubbles are present in Fig. 2b. The size of the bubbles, however, is similar in the two figures, suggesting bubble size is a function of the freezing method, not of the gas itself.

20 Figure 2c shows a histogram of the number of voxels containing various radiodensities, represented here as the ratio V_{LLR}/V_{VOXEL} , in the two water ice samples. A ratio of zero represents the average radiometric density for pure water ice, with values slightly greater or less than zero indicating noise in the sample images and reconstruction. Voxels containing only air comprise the smaller, second peak centered at approximately

Direct visualization of solute locations in laboratory ice samples

T. Hullar and
C. Anastasio

Title Page

Abstract

Introduction

Conclusions

References

Tables

Figures

◀

▶

◀

▶

Back

Close

Full Screen / Esc

Printer-friendly Version

Interactive Discussion



were frozen at similar temperatures, the morphologies are surprisingly different. As seen in Table 1, the fraction of voxels containing a LLR fraction $> 10\%$ is about five-fold less in the Freeze Chamber sample than the Freezer sample, while the fraction of voxels with an LLR concentration between 2 and 10% doubles. This finding indicates the freezing process in the freeze chamber is less likely to create large LLR inclusions than the freezer, with LLRs distributed more widely throughout the sample. Additionally, substantial amounts of solute were segregated towards the surface of the Freeze Chamber sample; presumably, the sample froze from the bottom and solutes were preferentially excluded from the advancing freezing front. However, the same process did not affect the air bubbles, which are well distributed throughout the sample. We believe these structural differences may be due to faster freezing in the Freeze Chamber sample, as the freeze chamber removes heat more quickly than the freezer because of direct contact between the bottom of the vial and the chilled base plate in the chamber. Figure S5 shows a sample prepared in the same way as in Fig. 3c, but with the metal plates in place in the freeze chamber, which surrounds the vial with metal rather than air. Here, we see similar bubble size and location as the sample frozen in the freeze chamber without the metal plates. However, unlike the sample frozen without plates in the freeze chamber, the solute distribution with plates shows no segregation towards the top of the sample, probably because the close proximity of the conductive metal plates removed heat from the sides and bottom of the sample simultaneously, similar to the Freezer case.

Results for a 1.0 mM CsCl sample prepared with the third freezing method – liquid nitrogen – is shown in Fig. 3e, with the full movie in Fig. S6. No air bubbles or significant solute inclusions are visible. However, as discussed earlier, some very small inclusions and air bubbles can be removed by the mathematical smoothing done by the reconstruction software, so very small features ($< \sim 80 \mu\text{m}$) may be present in the sample but lost in the reconstruction. A histogram of raw (i.e., not smoothed) greyscale values from the LN2 sample image does show some voxels contain concentrated solutes (Fig. 3g). As a further test of the possibility of solute inclusions in LN2 samples, we examined

Direct visualization of solute locations in laboratory ice samples

T. Hullar and
C. Anastasio

Title Page

Abstract

Introduction

Conclusions

References

Tables

Figures

◀

▶

◀

▶

Back

Close

Full Screen / Esc

Printer-friendly Version

Interactive Discussion



unreconstructed cross-sections of a 1.0 mM CsCl sample frozen in liquid nitrogen and imaged at $\sim 2 \mu\text{m}$ voxel resolution. As illustrated in Fig. S7 in the Supplement, there are some light (concentrated solute) and dark (air bubble) areas, suggesting some segregation of CsCl and air occurs even with rapid freezing (~ 30 s). However, this effect is barely visible in the quickly frozen liquid nitrogen sample (Fig. S7), and much more pronounced in the other two freezing methods (Figs. 3a and c).

Next, we examined the impact of solute on freezing morphology and solute location, by replacing CsCl with Rose Bengal, a large, organic molecule (see structure in Fig. S8). Figure 3f (movie: Fig. S9) shows a sample containing 1.0 mM Rose Bengal frozen in our freeze chamber. Using 1.0 mM Rose Bengal instead of 1.0 mM CsCl (Fig. 3c) gives a very different freezing pattern, with only a few small bubbles and a few areas of concentrated solute. While mathematical smoothing has likely eliminated some of the smaller structures, the overall sample morphology is quite different than that produced by the same concentration of CsCl. Interestingly, this change in solute alters not only the structure of solute inclusions, but also the size of the air bubbles. The exact reason for the change in morphology is unclear. CsCl is more polar than Rose Bengal, and could influence the movement of the polar water molecules into the forming ice matrix. Rose Bengal is also a relatively large organic molecule, much different than the ions of CsCl, and could therefore potentially modify the ice matrix due to its size. Finally, we note the thermodynamically predicted final concentration of solute ions at -10°C is 5.4 M; at this concentration CsCl should still be in solution, while a substantial portion of the Rose Bengal should have precipitated. Whether precipitated Rose Bengal is present as solids incorporated into the ice matrix or as precipitates in LLRs is not known.

Figure 3g shows the histogram for the 1.0 mM CsCl solutions frozen using each of the three freezing methods, as well as Milli-Q water ice frozen in a laboratory freezer. Unlike the images seen in Fig. 3a–f, where mathematical smoothing can eliminate small structures, the histograms include all the voxels in the sample. As discussed in Fig. 2c, water ice has two overlapping peaks, corresponding to air bubbles (left peak) and ice

Direct visualization of solute locations in laboratory ice samples

T. Hullar and
C. Anastasio

Title Page

Abstract

Introduction

Conclusions

References

Tables

Figures

◀

▶

◀

▶

Back

Close

Full Screen / Esc

Printer-friendly Version

Interactive Discussion



(right peak). Some voxels, shown in the “saddle” between the two peaks, contain both air bubbles and pure water ice, and will therefore have a greyscale value between air and ice. The Fig. 3g histogram clearly shows how CsCl tends to be present in larger LLR volumes in the Freezer sample, including some voxels that are almost completely composed of 2.7 M CsCl solution, with a maximum V_{LLR}/V_{VOXEL} of 0.9. This finding supports the idea of solutes segregating to concentrated LLRs during freezing, since if solutes were precipitating and forming solid inclusions in the bulk ice, the calculated ratio in a voxel could be higher than 1. The fact that the ratio gets close to, but never exceeds, 1 is consistent with our tricomponent model of air, relatively pure ice, and concentrated LLRs with a maximum concentration of 5.4 M total solute.

The increased number of air voxels on the left end of the curve for the 1.0 mM CsCl freezer sample represents voxels composed entirely of air. This number is larger than in the water sample, supporting the imaging findings that the presence of solute actually increases the size of air bubbles. For the Freeze Chamber and LN2 samples, the number of air bubbles is smaller, and voxels containing air are more likely to contain at least some fraction of ice or solute. For the Freeze Chamber sample, the histogram correlates with the images (Fig. 2c and d), with fewer voxels containing a large volume fraction of highly concentrated regions than in the Freezer sample. Finally, the liquid nitrogen results are nearly identical to water ice, although a few voxels with concentrated solute are present (also seen in Fig. S7).

The reproducibility of samples prepared on different days but using identical methods was quite good, with similar patterns seen for each replicate (Fig. S10). Each combination of freezing method and solute gave a distinct distribution of solute and air bubbles, suggesting these two variables are the primary factors influencing ice morphology.

Table 1 lists the calculated volume of each material domain and CsCl mass present, including all sample voxels, based on segmentation described in the Methods section. As seen in the images and histogram, the Freezer sample has the highest fraction (0.00019) of voxels containing 10% or more LLR volume, approximately 5 times greater than the Freeze Chamber sample. In contrast, the fraction of voxels with

Direct visualization of solute locations in laboratory ice samples

T. Hullar and
C. Anastasio

Title Page

Abstract

Introduction

Conclusions

References

Tables

Figures

◀

▶

◀

▶

Back

Close

Full Screen / Esc

Printer-friendly Version

Interactive Discussion



we believe it is related to how heat is removed from the sample during freezing. Because plastic conducts heat more poorly than water, ice, or glass, the vial walls act as insulators, forcing heat to be primarily removed from the bottom of the sample where the plastic vial contacts the chilled plate at the base of the freeze chamber. This may promote the formation of vertical air channels as the ice freezes upwards through the sample, rather than from the walls towards the interior in the glass vial sample.

We next examine the impact of freezing in plastic for a sample containing solutes. Figure S13 shows a 1.0 mM CsCl solution frozen in the freezer in a plastic vial; compared to the similarly treated sample frozen in a glass vial (Fig. 3a), the air bubbles and concentrated inclusions are smaller in the plastic vial. Interestingly, the air bubbles in the plastic vial CsCl Freezer sample do not show any of the elongation found when Milli-Q water is frozen in a plastic vial in the freeze chamber (Fig. S12), which may be related to the directional heat removal in the freeze chamber. Finally, once again using the freeze chamber, Fig. S14 shows 1.0 mM Rose Bengal frozen in plastic in the freeze chamber. Here, we see elongated solute inclusions; however, the air bubbles are not elongated.

We also performed several other experiments to examine the nature of LLRs. Figure 4 shows a cross-section of microCT images of the same sample (1.0 mM CsCl, frozen in laboratory freezer) at voxel resolutions of 16 μm (left) and 2 μm (right); the corresponding movies are in Fig. S15. The areas of light grey in the lower resolution image (16 μm voxel resolution), such as the area highlighted by the arrow, are likely areas where CsCl is present in small areas of concentrated LLRs bordered by pure water ice, although the voxel resolution does not show these features separately. As would be expected if freezing water effectively excludes solutes from the forming bulk ice matrix, the right hand image shows areas of concentrated LLRs adjacent to areas of pure water ice, supporting the idea discussed earlier that during freezing solutes are preferentially excluded from the forming ice matrix into small areas of concentrated solution. The higher resolution image in Fig. 4 also shows very clearly how the solutes in LLRs often wrap around the bubbles in the Freezer CsCl samples.

Direct visualization of solute locations in laboratory ice samples

T. Hullar and
C. Anastasio

[Title Page](#)[Abstract](#)[Introduction](#)[Conclusions](#)[References](#)[Tables](#)[Figures](#)[◀](#)[▶](#)[◀](#)[▶](#)[Back](#)[Close](#)[Full Screen / Esc](#)[Printer-friendly Version](#)[Interactive Discussion](#)

Direct visualization of solute locations in laboratory ice samples

T. Hullar and
C. Anastasio

Title Page

Abstract

Introduction

Conclusions

References

Tables

Figures

◀

▶

◀

▶

Back

Close

Full Screen / Esc

Printer-friendly Version

Interactive Discussion



Finally, Fig. 5 (and the accompanying movie in Fig. S16) gives further evidence supporting the idea that CsCl is contained in liquid-like regions in our ice samples. We placed a 1.0 mM CsCl sample (glass vial; Freezer) in the microCT sample holder set at -10°C and took images of the sample ($2\ \mu\text{m}$ voxel resolution, $X-Z$ plane) at 0, 11, and 22 h. The temperature gradient in the sample holder was measured later by placing a thermocouple sensor between the glass vial and the holder wall at various positions. The vertical temperature difference between the bottom and middle of the holder (approximately 1.7 cm, extending above and below the 1 cm height of the frozen sample in the vial) was 2.2°C , resulting in a gradient of $0.13^{\circ}\text{C mm}^{-1}$. As seen in the three images, the bright areas of CsCl move in the direction of the temperature gradient, towards the warmer top of the vial, at a rate of approximately $0.01\ \text{mm h}^{-1}$. In many cases, the solutes appear to be migrating around the surfaces of air bubbles, which are visible as darker grey spheres. While the air bubbles remain stationary in the ice matrix, the CsCl moves, consistent with the idea that solutes are present as a concentrated liquid-like solution, which can migrate either along the boundaries between air bubbles and the bulk ice, or possibly by melting into the bulk ice itself.

4 Implications and conclusions

Using microCT we directly visualized the locations of solute, gas, and bulk ice in laboratory-prepared ice samples. While the chemical concentrations we used are higher than those in clean polar samples, we expect that solutes in natural snow and ice might sometimes have similar, significant impacts on sample morphology, including the location and sizes of liquid-like regions and air bubbles.

Highlighting the sensitivity of ice structure to freezing conditions, we found a surprisingly large difference between samples prepared at freezing temperatures in an upright freezer (where the sample was surrounded by cold air) vs. our custom-built freeze chamber (where the sample sat on a cold plate). Samples frozen in liquid nitrogen, as expected, did not have the large air bubbles and LLR inclusions found in

Freezer or Freeze Chamber samples; nonetheless, we did find some evidence for the segregation of solutes into LLRs, even with the fast freezing of liquid nitrogen.

Cesium chloride and Rose Bengal impacted the ice sample structure differently; CsCl yielded larger air bubbles and solute inclusions compared to Rose Bengal. While the observed variations in the locations and sizes of solute inclusions might be expected for solutes of different polarity and size, the influence of solute on bubble morphology is more surprising. CsCl samples frozen in our laboratory freezer showed large LLRs, often wrapping around air bubbles. While QLLs at the surface ice–air interface of ice or snow are obviously in contact with atmospheric oxidants, the preferential collocation of internal LLRs and air bubbles represents a previously unrecognized air–ice interface. Depending on the chemistry occurring at this interface, the bubbles might be a source of oxidants and other gas-phase chemicals to internal solutes, and might have significant impacts for chemical transformations under certain conditions.

Our work here can help guide further investigations to understand the driving forces shaping snow and ice structures in the natural world, as well as the rate of chemical reactions in snow and ice. At the same time, our results suggest subtle changes in the preparation of laboratory ice samples can have significant impacts on the location of solutes in samples, requiring careful and consistent sample preparation to ensure meaningful results.

Acknowledgements. We thank Doug Rowland for microCT imaging assistance, David Paige (Paige Instruments) for constructing the temperature-controlled microCT sample chamber, and Bill Simpson and Peter Peterson for useful conversations and suggestions. We are grateful for funding from the National Science Foundation (grant CHE-1214121).

TCD

doi:10.5194/tc-2015-197

Direct visualization of solute locations in laboratory ice samples

T. Hullar and
C. Anastasio

Title Page

Abstract

Introduction

Conclusions

References

Tables

Figures

◀

▶

◀

▶

Back

Close

Full Screen / Esc

Printer-friendly Version

Interactive Discussion



References

- Barnes, P. R. F., Wolff, E. W., Mallard, D. C., and Mader, H. M.: SEM studies of the morphology and chemistry of polar ice, *Microsc. Res. Techniq.*, 62, 62–69, doi:10.1002/jemt.10385, 2003.
- 5 Barret, M., Domine, F., Houdier, S., Gallet, J. C., Weibring, P., Walega, J., Fried, A., and Richter, D.: Formaldehyde in the Alaskan Arctic snowpack: Partitioning and physical processes involved in air-snow exchanges, *J. Geophys. Res.-Atmos.*, 116, D00R03, doi:10.1029/2011jd016038, 2011.
- 10 Bartels-Rausch, T., Jacobi, H.-W., Kahan, T. F., Thomas, J. L., Thomson, E. S., Abbatt, J. P. D., Ammann, M., Blackford, J. R., Bluhm, H., Boxe, C., Domine, F., Frey, M. M., Gladich, I., Guzmán, M. I., Heger, D., Huthwelker, Th., Klán, P., Kuhs, W. F., Kuo, M. H., Maus, S., Moussa, S. G., McNeill, V. F., Newberg, J. T., Pettersson, J. B. C., Roeselová, M., and Sodeau, J. R.: A review of air–ice chemical and physical interactions (AICI): liquids, quasi-liquids, and solids in snow, *Atmos. Chem. Phys.*, 14, 1587–1633, doi:10.5194/acp-14-1587-2014, 2014.
- 15 Beine, H. J., Domine, F., Simpson, W., Honrath, R. E., Sparapani, R., Zhou, X. L., and King, M.: Snow-pile and chamber experiments during the Polar Sunrise Experiment “Alert 2000”: exploration of nitrogen chemistry, *Atmos. Environ.*, 36, 2707–2719, doi:10.1016/s1352-2310(02)00120-6, 2002.
- 20 Beine, H., Anastasio, C., Esposito, G., Patten, K., Wilkening, E., Domine, F., Voisin, D., Barret, M., Houdier, S., and Hall, S.: Soluble, light-absorbing species in snow at Barrow, Alaska, *J. Geophys. Res.-Atmos.*, 116, D14302, doi:10.1029/2011jd016181, 2011.
- Blanke, A., Beckmann, F., and Misof, B.: The head anatomy of *Epiophlebia superstes* (Odonata: Epiophlebiidae), *Org. Divers. Evol.*, 13, 55–66, doi:10.1007/s13127-012-0097-z, 2013.
- 25 Chen, S. and Baker, I.: Evolution of individual snowflakes during metamorphism, *J. Geophys. Res.-Atmos.*, 115, D21114, doi:10.1029/2010jd014132, 2010.
- Cheng, J., Soetjijto, C., Hoffmann, M. R., and Colussi, A. J.: Confocal fluorescence microscopy of the morphology and composition of interstitial fluids in freezing electrolyte solutions, *J. Phys. Chem. Lett.*, 1, 374–378, doi:10.1021/jz9000888, 2010.
- 30 Cho, H., Shepson, P. B., Barrie, L. A., Cowin, J. P., and Zaveri, R.: NMR investigation of the quasi-brine layer in ice/brine mixtures, *J. Phys. Chem. B*, 106, 11226–11232, doi:10.1021/jp020449+, 2002.

Direct visualization of solute locations in laboratory ice samples

T. Hullar and
C. Anastasio

Title Page

Abstract

Introduction

Conclusions

References

Tables

Figures

◀

▶

◀

▶

Back

Close

Full Screen / Esc

Printer-friendly Version

Interactive Discussion



Direct visualization of solute locations in laboratory ice samplesT. Hullar and
C. Anastasio

Title Page

Abstract

Introduction

Conclusions

References

Tables

Figures

◀

▶

◀

▶

Back

Close

Full Screen / Esc

Printer-friendly Version

Interactive Discussion



- Chu, L. and Anastasio, C.: Formation of hydroxyl radical from the photolysis of frozen hydrogen peroxide, *J. Phys. Chem. A*, 109, 6264–6271, doi:10.1021/jp051415f, 2005.
- Dibb, J. E. and Arsenault, M.: Shouldn't snowpacks be sources of monocarboxylic acids?, *Atmos. Environ.*, 36, 2513–2522, 2002.
- 5 Domine, F. and Shepson, P. B.: Air–snow interactions and atmospheric chemistry, *Science*, 297, 1506–1510, 2002.
- Domine, F., Albert, M., Huthwelker, T., Jacobi, H.-W., Kokhanovsky, A. A., Lehning, M., Picard, G., and Simpson, W. R.: Snow physics as relevant to snow photochemistry, *Atmos. Chem. Phys.*, 8, 171–208, doi:10.5194/acp-8-171-2008, 2008.
- 10 Douglas, T. A. and Sturm, M.: Arctic haze, mercury and the chemical composition of snow across northwestern Alaska, *Atmos. Environ.*, 38, 805–820, doi:10.1016/j.atmosenv.2003.10.042, 2004.
- Evans, N. J., McInnes, B. I. A., Squelch, A. P., Austin, P. J., McDonald, B. J., and Wu, Q. H.: Application of X-ray micro-computed tomography in (U-Th)/He thermochronology, *Chem. Geol.*, 15 257, 101–113, doi:10.1016/j.chemgeo.2008.08.021, 2008.
- Grannas, A. M., Jones, A. E., Dibb, J., Ammann, M., Anastasio, C., Beine, H. J., Bergin, M., Bottenheim, J., Boxe, C. S., Carver, G., Chen, G., Crawford, J. H., Dominé, F., Frey, M. M., Guzmán, M. I., Heard, D. E., Helmig, D., Hoffmann, M. R., Honrath, R. E., Huey, L. G., Hutterli, M., Jacobi, H. W., Klán, P., Lefer, B., McConnell, J., Plane, J., Sander, R., Savarino, J., 20 Shepson, P. B., Simpson, W. R., Sodeau, J. R., von Glasow, R., Weller, R., Wolff, E. W., and Zhu, T.: An overview of snow photochemistry: evidence, mechanisms and impacts, *Atmos. Chem. Phys.*, 7, 4329–4373, doi:10.5194/acp-7-4329-2007, 2007.
- Haynes, W. M. E.: *CRC Handbook of Chemistry and Physics*, 95th Edn., CRC Press, Boca Raton, Florida, USA, 2014.
- 25 Heggli, M., Kochle, B., Matzl, M., Pinzer, B. R., Riche, F., Steiner, S., Steinfeld, D., and Schneebeli, M.: Measuring snow in 3-D using X-ray tomography: assessment of visualization techniques, *Ann. Glaciol.*, 52, 231–236, 2011.
- Hullar, T. and Anastasio, C.: Yields of hydrogen peroxide from the reaction of hydroxyl radical with organic compounds in solution and ice, *Atmos. Chem. Phys.*, 11, 7209–7222, doi:10.5194/acp-11-7209-2011, 2011.
- 30 Hullar, T., Paige, D. F., Rowland, D. J., and Anastasio, C.: Compact cold stage for micro-computerized tomography imaging of chilled or frozen samples, *Rev. Sci. Instrum.*, 85, 043708, doi:10.1063/1.4871473, 2014.

**Direct visualization of
solute locations in
laboratory ice
samples**T. Hullar and
C. Anastasio

Title Page

Abstract

Introduction

Conclusions

References

Tables

Figures

◀

▶

◀

▶

Back

Close

Full Screen / Esc

Printer-friendly Version

Interactive Discussion

- Jacobi, H. W., Bales, R. C., Honrath, R. E., Peterson, M. C., Dibb, J. E., Swanson, A. L., and Albert, M. R.: Reactive trace gases measured in the interstitial air of surface snow at Summit, Greenland, *Atmos. Environ.*, 38, 1687–1697, doi:10.1016/j.atmosenv.2004.01.004, 2004.
- Jacobi, H. W., Annor, T., and Quansah, E.: Investigation of the photochemical decomposition of nitrate, hydrogen peroxide, and formaldehyde in artificial snow, *J. Photochem. Photobiol. A*, 179, 330–338, doi:10.1016/j.jphotochem.2005.09.001, 2006.
- Kahan, T. F. and Donaldson, D. J.: Photolysis of polycyclic aromatic hydrocarbons on water and ice surfaces, *J. Phys. Chem. A*, 111, 1277–1285, doi:10.1021/jp066660t, 2007.
- Kahan, T. F. and Donaldson, D. J.: Benzene photolysis on ice: implications for the fate of organic contaminants in the winter, *Environ. Sci. Technol.*, 44, 3819–3824, doi:10.1021/es100448h, 2010.
- Kahan, T. F., Zhao, R., Jumaa, K. B., and Donaldson, D. J.: Anthracene photolysis in aqueous solution and ice: Photon flux dependence and comparison of kinetics in bulk ice and at the air–ice interface, *Environ. Sci. Technol.*, 44, 1302–1306, doi:10.1021/es9031612, 2010.
- Kurkova, R., Ray, D., Nachtigallova, D., and Klan, P.: Chemistry of small organic molecules on snow grains: the applicability of artificial snow for environmental studies, *Environ. Sci. Technol.*, 45, 3430–3436, doi:10.1021/es104095g, 2011.
- Lomonaco, R. W., Chen, S., and Baker, I.: Characterization of porous snow with SEM and Micro CT, *Microsc. Microanal.*, 15, 1110–1111, doi:10.1017/s1431927609093313, 2009.
- Lomonaco, R. W., Albert, M., and Baker, I.: Microstructural evolution of fine-grained layers through the firn column at Summit, Greenland, *J. Glaciol.*, 57, 755–762, 2011.
- Neckers, D. C.: Rose Bengal, *J. Photochem. Photobiol. A*, 47, 1–29, doi:10.1016/1010-6030(89)85002-6, 1989.
- NIH: PubChem Open Chemistry Database, available at: <http://pubchem.ncbi.nlm.nih.gov>, last access: 7 July 2015.
- NIST: X-ray Form Factor, Attenuation, and Scattering Tables, available at: <http://physics.nist.gov/PhysRefData/FFast/html/form.html>, last access: 5 July 2015.
- Obbard, R. W., Troderman, G., and Baker, I.: Imaging brine and air inclusions in sea ice using micro-X-ray computed tomography, *J. Glaciol.*, 55, 1113–1115, 2009.
- Phillips, G. J. and Simpson, W. R.: Verification of snowpack radiation transfer models using actinometry, *J. Geophys. Res.-Atmos.*, 110, D08306 doi:10.1029/2004jd005552, 2005.
- Ram, K. and Anastasio, C.: Photochemistry of phenanthrene, pyrene, and fluoranthene in ice and snow, *Atmos. Environ.*, 43, 2252–2259, doi:10.1016/j.atmosenv.2009.01.044, 2009.

- Rosenthal, W., Saleta, J., and Dozier, J.: Scanning electron microscopy of impurity structures in snow, *Cold Reg. Sci. Technol.*, 47, 80–89, doi:10.1016/j.coldregions.2006.08.006, 2007.
- Sumner, A. L. and Shepson, P. B.: Snowpack production of formaldehyde and its effect on the Arctic troposphere, *Nature*, 398, 230–233, 1999.
- 5 Yang, Q., Mayewski, P. A., Linder, E., Whitlow, S., and Twickler, M.: Chemical species spatial distribution and relationship to elevation and snow accumulation rate over the Greenland Ice Sheet, *J. Geophys. Res.-Atmos.*, 101, 18629–18637, doi:10.1029/96jd01061, 1996.

Direct visualization of solute locations in laboratory ice samples

T. Hullar and
C. Anastasio

Title Page

Abstract

Introduction

Conclusions

References

Tables

Figures

◀

▶

◀

▶

Back

Close

Full Screen / Esc

Printer-friendly Version

Interactive Discussion



Direct visualization of solute locations in laboratory ice samples

T. Hullar and
C. Anastasio

Table 1. Sample volumes and fractions by material type.

Sample	Initial solution volume (μL)	Total CsCl mass (μg)	Gas	Volume (mm ³) ^a			Gas	Volume Fraction ^{a,b}			CsCl Mass Fraction ^{a,c}		
				Water ice	LLR 2–10%	LLR > 10%		Water ice	LLR 2–10%	LLR > 10%	Water ice	LLR 2–10%	LLR > 10%
MilliQ water													
Freezer	500	0	5.96	430	0	0	0.014	0.986	0	0	–	–	–
Freezer, degassed	500	0	3.23	432	0	0	0.007	0.993	0	0	–	–	–
1 mM CsCl													
Freezer	750	126.3	5.07	716	2.35	0.141	0.007	0.990	0.003	0.00019	0.651	0.233	0.116
Freeze chamber	500	84.2	5.55	473	2.67	0.0176	0.012	0.983	0.006	0.000037	0.640	0.346	0.014
Liquid nitrogen	750	126.3	0	725	1.50	0	0	0.998	0.002	0	0.879	0.121	0.000

^a “Gas” is defined as having a greyscale value of < 3996, “Water ice” is defined as containing < 2% liquid-like region (LLR), “LLR 2–10%” is water ice containing an LLR fraction of between 2 and 10%, and “LLR > 10%” is water ice containing > 10% LLR. The original sample volume (either 500 or 750 μL) is not fully captured in the volumes reported here. The segmentation process eliminates some of the lower part of the sample, reducing the reported volume somewhat.

^b Fraction of imaged sample volume (not initial solution volume). See text for details.

^c Fraction of total CsCl mass present in each domain. Because the mass of CsCl present in the water ice compartment could not be determined directly, we assumed any mass not present in either the LLR 2–10% or LLR > 10% domain is present in the water ice domain.

Direct visualization of solute locations in laboratory ice samples

T. Hullar and
C. Anastasio

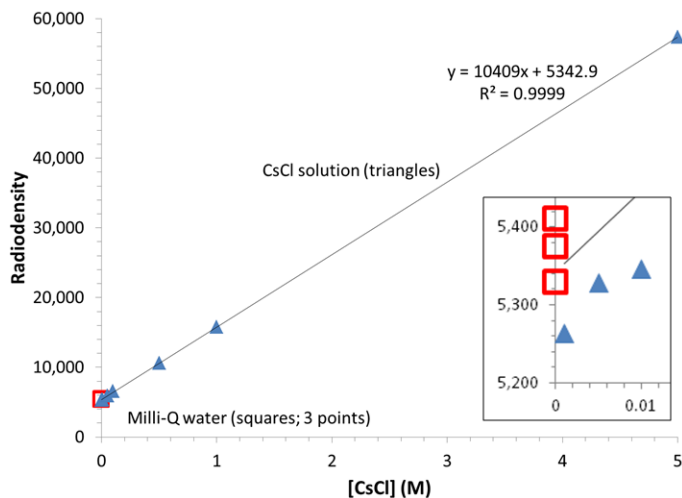


Figure 1. Radiodensity of pure water (red open squares, three data points) and of aqueous solutions containing CsCl (blue triangles).

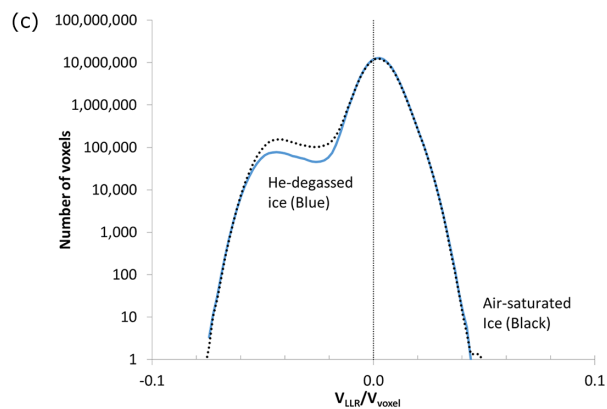
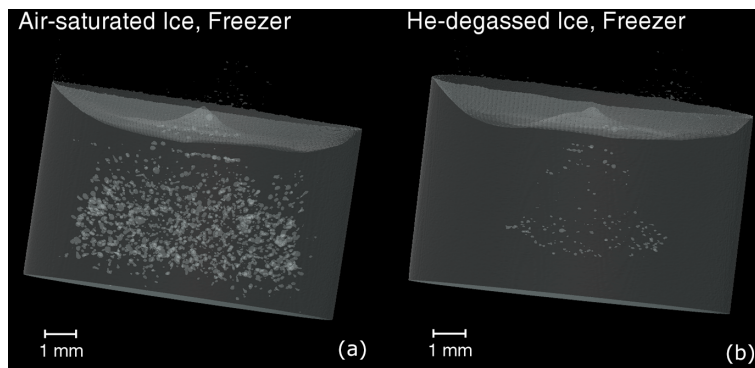
[Title Page](#)[Abstract](#)[Introduction](#)[Conclusions](#)[References](#)[Tables](#)[Figures](#)[◀](#)[▶](#)[◀](#)[▶](#)[Back](#)[Close](#)[Full Screen / Esc](#)[Printer-friendly Version](#)[Interactive Discussion](#)

TCD

doi:10.5194/tc-2015-197

Direct visualization of solute locations in laboratory ice samples

T. Hullar and
C. Anastasio



Title Page

Abstract

Introduction

Conclusions

References

Tables

Figures

◀

▶

◀

▶

Back

Close

Full Screen / Esc

Printer-friendly Version

Interactive Discussion



Figure 2. Reconstructed images **(a, b)** and histogram **(c)** of water ice samples frozen in a laboratory freezer, imaged using microCT ($\sim 16 \mu\text{m}$ voxel size) and segmented to show air bubbles (light grey) and the bulk ice matrix (darker grey). The glass sample vial is not shown. The ice in **(a)** was made using air-saturated water, while that in **(b)** was made with water degassed with helium for 30 min before freezing. **(c)** shows the distributions of the radiodensities within the two samples, expressed as the fraction of each voxel that would be occupied by a liquid-like region (LLR) assuming the total solute concentration is determined by freezing point depression (i.e., 5.4 M at -10°C , Cho et al., 2002).

Direct visualization of solute locations in laboratory ice samples

T. Hullar and
C. Anastasio

[Title Page](#)[Abstract](#)[Introduction](#)[Conclusions](#)[References](#)[Tables](#)[Figures](#)[|◀](#)[▶|](#)[◀](#)[▶](#)[Back](#)[Close](#)[Full Screen / Esc](#)[Printer-friendly Version](#)[Interactive Discussion](#)

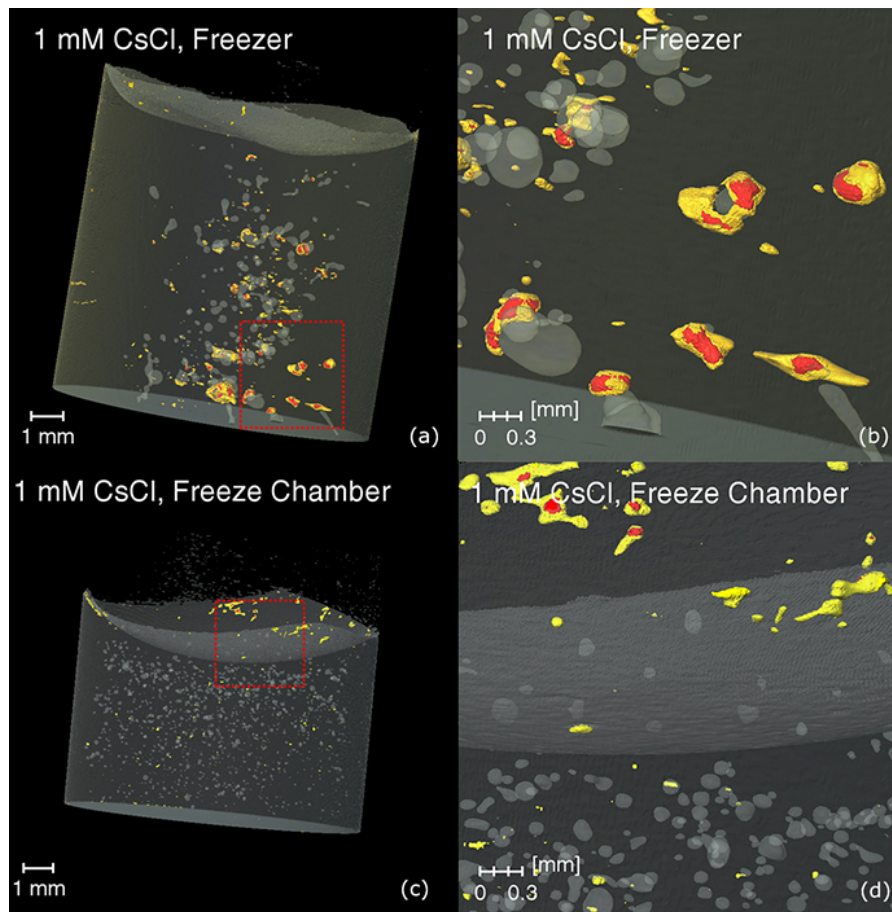


Figure 3.

Direct visualization of solute locations in laboratory ice samples

T. Hullar and C. Anastasio

Title Page	
Abstract	Introduction
Conclusions	References
Tables	Figures
◀	▶
◀	▶
Back	Close
Full Screen / Esc	
Printer-friendly Version	
Interactive Discussion	

Direct visualization of solute locations in laboratory ice samples

T. Hullar and
C. Anastasio

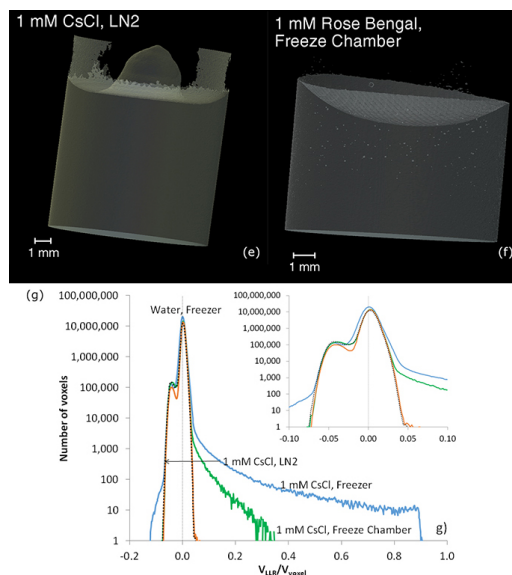


Figure 3. Reconstructed images and histograms of ice samples frozen using three freezing methods and with two different solutes. Samples were imaged using a $\sim 16 \mu\text{m}$ voxel size and segmented to show air bubbles (light grey), the bulk ice matrix (darker grey), voxels where V_{LLR}/V_{VOXEL} is between 2 and 10% (orange) and where $V_{LLR}/V_{VOXEL} > 10\%$ (red). The sample vial is not shown. **(a)** 1.0 mM CsCl solution frozen in freezer. **(b)** blowup of the area in **(a)** identified by the dashed red square. **(c)** 1.0 mM CsCl solution frozen in freeze chamber. **(d)** Blowup of the dashed-line area of **(c)**. **(e)** 1.0 mM CsCl solution frozen in liquid nitrogen. No air bubbles or inclusions are visible at this scale. **(f)** 1.0 mM Rose Bengal solution frozen in freeze chamber. **(g)** histogram showing distribution of voxel counts for the CsCl and Milli-Q water ice samples shown above: water ice frozen in freezer, black dotted line; 1.0 mM CsCl frozen in LN2, orange line; 1.0 mM CsCl frozen in freezer, blue line; 1.0 mM CsCl, frozen in freeze chamber, green line. The inset shows an expanded view from $V_{LLR}/V_{VOXEL} = -0.1$ to 0.1.

Direct visualization of solute locations in laboratory ice samples

T. Hullar and
C. Anastasio

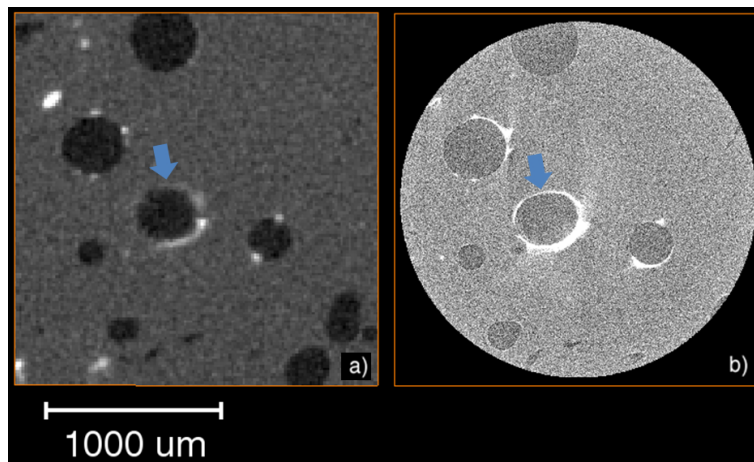


Figure 4. Side-by-side micro CT cross sections of the same sample (1.0 mM CsCl, frozen in laboratory freezer) imaged at approximately 16 μm (**a**) and 2 μm (**b**) voxel sizes. Lighter tones indicate areas of higher radiodensity, i.e., higher solute amounts. The scale bar applies to both images.

[Title Page](#)[Abstract](#)[Introduction](#)[Conclusions](#)[References](#)[Tables](#)[Figures](#)[◀](#)[▶](#)[◀](#)[▶](#)[Back](#)[Close](#)[Full Screen / Esc](#)[Printer-friendly Version](#)[Interactive Discussion](#)

Direct visualization of solute locations in laboratory ice samples

T. Hullar and
C. Anastasio

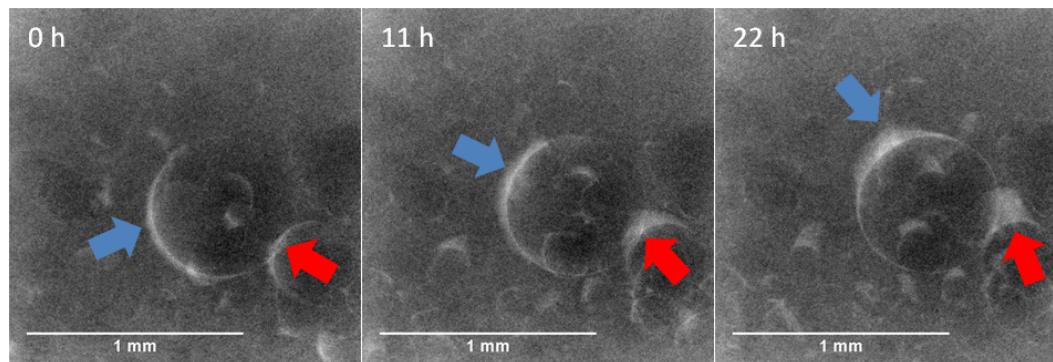


Figure 5. X-ray images of a 1.0 mM CsCl ice (laboratory freezer, voxel resolution $\sim 2 \mu\text{m}$) after 0, 11, and 22 h in the CT sample chamber. Lighter tones indicate areas of higher radiodensity (e.g., greater CsCl amounts). Air bubbles are visible as darker gray spheres. The temperature of the sample holder was set at -10°C , but the top of the sample was approximately 1.3°C warmer than the bottom, corresponding to a temperature gradient of approximately $0.13^\circ\text{C mm}^{-1}$. Arrows highlight two of the areas where CsCl moves along the direction of the temperature gradient.

[Title Page](#)[Abstract](#)[Introduction](#)[Conclusions](#)[References](#)[Tables](#)[Figures](#)[◀](#)[▶](#)[◀](#)[▶](#)[Back](#)[Close](#)[Full Screen / Esc](#)[Printer-friendly Version](#)[Interactive Discussion](#)